Numerical Simulation of Conjugate Laminar Mixed Convection in a Vented Prismatic Room

Rashadul Islam Ritu, Enamul Hasan Rozin, Sumon Saha and Sheikh Mohammad Shavik
Department of Mechanical Engineering
Bangladesh University of Engineering and Technology
Dhaka-1000, Bangladesh
rashadulislam150@gmail.com, enamulrozin4@gmail.com, sumonsaha@me.buet.ac.bd,
shavik@me.buet.ac.bd

Abstract

In this study, conjugate laminar mixed convection heat transfer inside a vented prismatic shaped room has been investigated. According to the cooler's position, three different types of configurations are considered. Cold air enters the room through the inlet and exits through a ventilator located at the roof. The bottom wall is considered adiabatic, and all the outer sidewalls are at a constant ambient temperature. The outer roof of the room is exposed to the sun, thus having a constant heat flux. The set of governing equations with boundary conditions have been solved via the finite element method. A parametric study is conducted for Richardson numbers ranging from 0.1 to 10. The average Nusselt number at the solid-fluid interfaces, the temperature distribution effectiveness, and the air domain's average temperature are evaluated to make a quantitative comparison of different parameters and configurations. The room's thermal and flow field distributions are presented through isotherm contour, heatline, and streamline plots. It is found that when the cooler is placed at the bottom position inside the room, the average fluid temperature of the room becomes lowest, and the temperature distribution effectiveness also becomes maximum for any Richardson number, thus indicates better thermal performance.

Keywords
Vented room, mixed convection, finite element method, laminar flow, prismatic enclosure.

1. Introduction
Designing a room for either industrial purposes or personal use includes lots of parameters to merge. One of the important concerns is to predict the heat transfer inside the room. The quantity of heat generated inside the room can cause thermal discomfort and can also affect the performance of the occupants inside. Appropriate positioning of the air conditioning and ventilation systems not only saves expenses, but also boosts up the performance of the occupants inside the room.
It is necessary to understand the requirements of the indoor environment of buildings to ensure thermal comfort. The indoor environment mostly depends on the heat transfer through the buoyancy-driven flow of air. However, for better air quality and comfort, the artificial air conditioning system is also used, which influences the flow field and temperature. This combined natural and forced convection heat transfer that arises in indoor spaces is also found in many engineering applications such as electronic chips, heat exchangers, food processing, etc.

1.1 Literature Review
Different studies have been done considering the effect of fluid flow and heat transfer in a prismatic enclosure. Manca et al.(2003) numerically derived that opposing forced flow configuration in a partially open cavity has the highest heat transfer rate for various aspect ratios. Later on, the same authors (Manca et al. (2006)) have carried out an experimental investigation that was in very good agreement with the stream function fields presented in the previous one. Alam et al. (2016) investigated the rate of heat transfer, velocity, and average temperature for two cases; uniformly heated bottom wall and linearly heated bottom wall in a prismatic cavity. They evaluated that for a higher value of Rayleigh number, the heat transfer rate is maximum with the help of heatlines, and for a uniformly heated bottom wall, higher velocity and average temperature can be achieved than the linearly heated bottom wall. Walid et al. (2016) studied natural convection heat transfer in a prismatic enclosure. They showed that the cavity's aspect ratio has a significant effect on the flow and thermal field, and the effect of a small Rayleigh number value is

insignificant. Hasan et al. (2019) investigated conjugate heat transfer and entropy generation for different heating conditions at the bottom wall of a prismatic enclosure. They emphasized on heatlines in determining the rate of heat transfer.

The enhancement of the heat transfer rate can be achieved by varying Reynolds number, but evaluating different geometric configuration is necessary for making it more thermally efficient. Many researchers already performed experimental and numerical investigations to find out the best possible configuration for a particular geometry. Rahman et al. (2007) examined a total of nineteen inlet locations. They evaluated the inlet's fixed location for which the heat transfer was higher for a range of Reynolds number from 50 to 200. Several studies have been conducted to evaluate the best cooling performance inside a cavity. Hence Aminossadati and Behzad (2009) performed a numerical study to determine the best cooling performance depending upon the location of a discrete heat source. However, using a pulsating flow, heat transfer can be largely enhanced. Notably, Shivran et al. (2017) used a square cavity and evaluated the optimized geometry by applying four different Richardson numbers and volume fractions. They used Cu-water as nanofluid and concluded that heat transfer was maximum for a fixed position of inlet and outlet vents. Caroazza (2018) referred to a suitable configuration of a vented cavity having a particular range of aspect ratio (H/D equals to 0.1, L/D varies from 0.5 to 4, where H, L, D refer to height of the canal, length of the recess and height of the recess of the cavity respectively), and concluded that Reynolds number was the most critical parameter to control the heat transfer inside the cavity. He also suggested that it was better to provide a heated surface configuration, which was in the same direction as the air inlet into the tube, to achieve greater heat dissipation. Besides, variating the inlet height can be a great idea to increase efficiency. Because of the position of the inlet, the entering air can get enough time to circulate and to cool the cavity.

A significant number of experimental and numerical work was carried out in recent years to understand the flow and thermal behavior of the indoor environment. Most of these works were considered in a rectangular room. Gan and Awbi (1994) performed a CFD simulation in an indoor room and evaluated the spread of indoor pollutants such as CO_2. Raji and Hasnaoui (2000) numerically analyzed the heat transfer and fluid flow characteristics inside a vented cavity subjected to constant heat flux on the left wall. Hinojosa et al. (2016) showed both experimental and numerical results of heat transfer and fluid flow in a ventilated room. Stavridou and Prinos (2017) conducted a CFD simulation in a naturally ventilated room with a localized heat source. Koufi et al. (2017) examined turbulent mixed convection for an open cavity with four different inlet-outlet configurations and reported the best configuration with maximum efficiency.

1.2 Objectives

From the existing literature related to this field, it can be said that the thermal and flow modeling inside a vented prismatic enclosure with cooler and heat flux on the the inclined walls has not been studied yet. Therefore, the aim of this present work is to observe the heat dissipation for different cooler positions and generate heatlines for a better understanding of the heat distribution inside the prismatic room and find an optimized cooler's position.

2. Model Description

2.1 Geometric Details

The schematic representation of the present model is depicted in figure 1 in Cartesian coordinate system associated with boundary the conditions and corresponding dimensions as shown in figure 1. Three different cases are considered. For each case, simulation is carried out in a prismatic room with an adiabatic bottom wall, while the sidewalls are kept at a constant temperature, T_∞ and the inclined top walls are kept at a constant heat flux, q, representing the exposure of solar heat flux. Air enters through the cooler at cold temperature T_c and velocity u_i. The ventilator is placed at a position, where the flow exits from the inside space. The thermal conductivity and thickness of different materials at the side and the inclined walls are given in table 1.

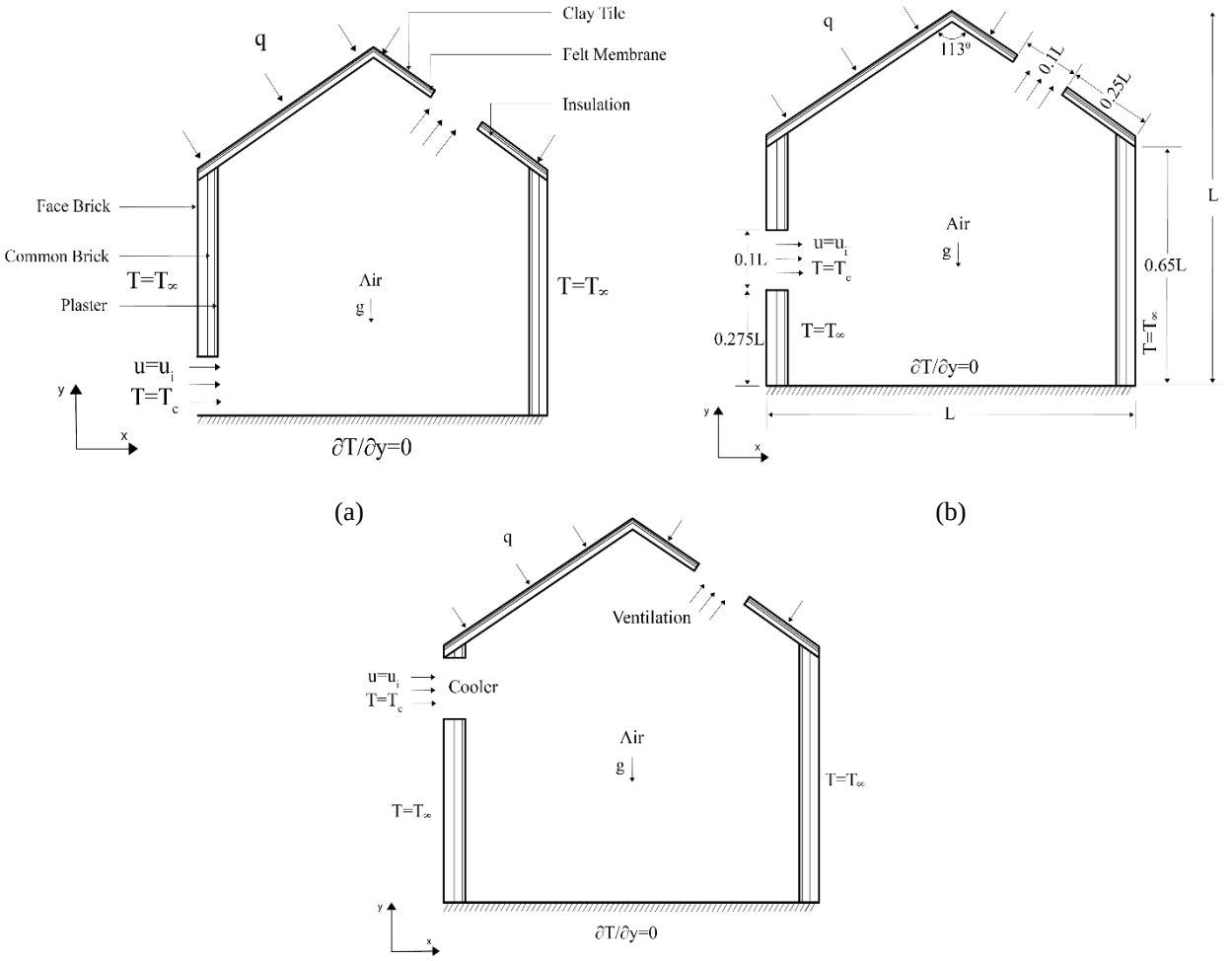

Figure 1. Schematic diagram of three different geometries based on inlet position at (a) bottom inlet (case 1), (b) middle inlet (case 2) and (c) top inlet (case 3) configurations

2.2 Governing Equations and Boundary conditions:

Here, the flow is considered to be to be two-dimensional, incompressible, Newtonian, and laminar. Density variation of air is dealt with Boussinesq approximation. Other thermophysical air properties like density, dynamic viscosity, specific heat capacity, and thermal conductivity are constant with temperature variation. Heat transfer by radiation is also neglected. Based on the assumptions stated above, the governing dimensional Navier-Stokes and energy equations for this simplified, steady-state model can be written as follows:

$$\frac{\partial u}{\partial x}+\frac{\partial v}{\partial y}=0\,, \tag{1}$$

$$\rho\left(u\frac{\partial u}{\partial x}+v\frac{\partial u}{\partial y}\right)=-\frac{\partial p}{\partial x}+\mu\left(\frac{\partial^2 u}{\partial x^2}+\frac{\partial^2 u}{\partial y^2}\right), \tag{2}$$

$$\rho\left(u\frac{\partial v}{\partial x}+v\frac{\partial v}{\partial y}\right)=-\frac{\partial p}{\partial y}+\mu\left(\frac{\partial^2 v}{\partial x^2}+\frac{\partial^2 v}{\partial y^2}\right)+\rho g\beta\left(T-T_c\right), \tag{3}$$

$$\rho C_p\left(u\frac{\partial T}{\partial x}+v\frac{\partial T}{\partial y}\right)=k\left(\frac{\partial^2 T}{\partial x^2}+\frac{\partial^2 T}{\partial y^2}\right). \tag{4}$$

$$k_s\left(\frac{\partial^2 T_s}{\partial x^2}+\frac{\partial^2 T_s}{\partial y^2}\right)=0. \tag{5}$$

Following non-dimensional scales are used to convert the equations (1) –(5) into dimensionless forms:

$$X=\frac{x}{L}, Y=\frac{y}{L}, U=\frac{u}{u_i}, V=\frac{v}{u_i}, P=\frac{p}{\rho u_i^2}, \theta=\frac{T-T_c}{qL/k_{air}}, \theta_s=\frac{T_s-T_c}{qL/k_{air}}. \tag{6}$$

By using the above scales, equations (1)-(5) can transform into the following non-dimensional governing equations.

$$\frac{\partial U}{\partial X}+\frac{\partial V}{\partial Y}=0, \tag{7}$$

$$U\frac{\partial U}{\partial X}+V\frac{\partial U}{\partial Y}=-\frac{\partial P}{\partial X}+\frac{1}{Re}\left(\frac{\partial^2 U}{\partial X^2}+\frac{\partial^2 U}{\partial Y^2}\right), \tag{8}$$

$$U\frac{\partial V}{\partial X}+V\frac{\partial V}{\partial Y}=-\frac{\partial P}{\partial Y}+\frac{1}{Re}\left(\frac{\partial^2 V}{\partial X^2}+\frac{\partial^2 V}{\partial Y^2}\right)+Ri\theta, \tag{9}$$

$$U\frac{\partial \theta}{\partial X}+V\frac{\partial \theta}{\partial Y}=\frac{1}{RePr}\left(\frac{\partial^2 \theta}{\partial X^2}+\frac{\partial^2 \theta}{\partial Y^2}\right), \tag{10}$$

$$\frac{\partial^2 \theta_S}{\partial X^2}+\frac{\partial^2 \theta_S}{\partial Y^2}=0. \tag{11}$$

Here L is the base length, X and Y are the axis of the non-dimensional coordinate system, θ is the non-dimensional temperature of the air, θ_s is the non-dimensional temperature of solid materials, U and V are the non-dimensional velocity components, P is the non-dimensional pressure, x and y are the axis of the cartesian coordinate system, T is the fluid temperature, u and v are the velocity components, p is the dimensional pressure. ρ is the density of air and k_{air}, is the thermal conductivity of air. Reynolds number, Richardson number, Grashof number, Prandtl number are used in the governing equations, which are defined as follows:

$$Re=\frac{u_i L}{\nu}, Ri=\frac{Gr}{Re^2}, Gr=\frac{g\beta q L^4}{k_{air}\nu^2}, Pr=\frac{\nu}{\alpha}, \tag{12}$$

where, β is the coefficient of thermal expansion of air, ν is the kinematic viscosity of air, α is the thermal diffusivity of air, and g is the gravitational acceleration. The Prandtl number of air is taken as 0.71. The thermal conductivity of air is equal to $k_{air}=0.02624$ W/m.K. Table 1 displays the thermal conductivity of other wall materials at the ambient temperature used in the model. Table 2 lists the non-dimensional boundary conditions.

Table 1. Dataset for thermal conductivity and thickness of solid materials and composites

Materials	Thickness	Thermal Conductivity (W/m.K)
Face brick	0.022L	1.333
Common brick	0.022L	0.727
Plaster	0.0044L	0.7277
Clay Tile	0.0043L	0.571
Felt	0.0022L	0.19
Insulation	0.011L	0.043

Table 2. Non- dimensional boundary conditions.

Boundary wall	Thermal Field	Velocity Field
Bottom Wall	$\frac{\partial \theta}{\partial Y}=0$	$U=V=0$
Left and Right Walls	$\theta=0.5$	$U=V=0$
Inclined Walls	$\frac{\partial \theta}{\partial n}=-1$	$U=V=0$

Inlet	$\theta = 0$	$U = 1$, $V = 0$
Outlet	$\frac{\partial \theta}{\partial n} = 0$	$\frac{\partial U}{\partial n} = 0$, $\frac{\partial V}{\partial n} = 0$
Solid-Solid Interface	$\left(\frac{\partial \theta}{\partial n}\right)_{solid} = R_c^{'}\left(\frac{\partial \theta}{\partial n}\right)_{solid}$	$U = V = 0$
Solid-Fluid Interface	$\left(\frac{\partial \theta}{\partial n}\right)_{fluid} = R_c\left(\frac{\partial \theta}{\partial n}\right)_{solid}$	$U = V = 0$

Here, R_c the ratio of thermal conductivity of solid and air and $R_c^{'}$ is the ratio of thermal conductivity of adjacent solid materials.

2.3 Average Nusselt Number

Average Nusselt number, a heat transfer performance parameter, can be calculated at the solid-fluid interface along the inclined walls and right walls respectively, which are defined as follows:

$$Nu_r = -\frac{\int_0^{S^{'}} \frac{\partial \theta}{\partial X} ds^{'}}{\int \theta ds^{'}},\ Nu_t = -\frac{\int_0^{S} \frac{\partial \theta}{\partial n} ds}{\int \theta ds}. \tag{13}$$

where Nu_t and Nu_r are the average Nusselt number along the inclined walls and the right walls, respectively. Also, $S^{'}$ is the length of the wall along the right solid-fluid wall interfaces and S is the length of the wall along the top inclined solid-fluid wall interfaces.

2.4 Average Temperature

Another performance parameter is the average fluid temperature evaluated in the fluid domain, which is calculated as follows:

$$\theta_{avg} = \frac{1}{A}\int_A \theta dA. \tag{14}$$

where A is the dimensionless area of the fluid domain.

2.5 Temperature Distribution Effectiveness

For an efficient room ventilation system, the temperature has to distribute uniformly. To evaluate how effectively the temperature is distributed across the room, temperature distribution effectiveness ε_T is calculated (Gan and Awbi, [1994]) which is defined as follows:

$$\varepsilon_T = \frac{\theta_{out} - \theta_{in}}{\theta_{avg} - \theta_{in}}. \tag{15}$$

Here, θ_{out} is the average outlet temperature, θ_{in} is the average inlet temperature, and θ_{avg} is the mean or average temperature of the air domain defined in equation (14).

2.6 Stream Function

The non-dimensional stream function which is used to visualize fluid flow pattern is related to the dimensionless velocity components U and V for two-dimensional flow such that

$$U = \frac{\partial \psi}{\partial Y},\ \mathrm{V} = -\frac{\partial \psi}{\partial X}, \tag{16}$$

Which generates a Poisson differential equation given as:

$$\frac{\partial^2 \psi}{\partial X^2}+\frac{\partial^2 \psi}{\partial Y^2}=\frac{\partial}{\partial Y}(U\theta)-\frac{\partial}{\partial X}(V\theta) \tag{17}$$

2.7 Heat Function

The heat energy flow across the fluid domain can be visualized by the heat function (Π). The heat function mainly consists of convective and conductive heat fluxes and satisfies the steady energy balance equation. In this study, the dimensionless convective fluxes are $U\theta$, $V\theta$ and dimensionless conductive fluxes $-\frac{1}{RePr}\frac{-\partial\theta}{\partial X}$, $-\frac{1}{RePr}\frac{\partial\theta}{\partial Y}$. The dimensionless heat function is related to conductive fluxes and convective fluxes by the following equations:

$$\frac{\partial \Pi}{\partial Y}=U\theta-\frac{1}{RePr}\frac{\partial\theta}{\partial X},\quad -\frac{\partial \Pi}{\partial X}=V\theta-\frac{1}{RePr}\frac{\partial\theta}{\partial Y}. \tag{18}$$

Equation (18) yields a Poisson equation of the form:

$$\frac{\partial^2 \Pi}{\partial X^2}+\frac{\partial^2 \Pi}{\partial Y^2}=\frac{\partial}{\partial Y}(U\theta)-\frac{\partial}{\partial X}(V\theta). \tag{19}$$

3 Numerical Procedure

The non-dimensional governing equations with corresponding boundary conditions are solved using the finite element method. The whole solid and fluid domain is discretized into a finite number of triangular elements. A relatively fine mesh is applied at the boundaries.

3.1 Grid Refinement Test

A grid refinement test is done, which is shown in table 3, to get a more accurate result with less computational time.

Table 3. Grid refinement test for case 1, $Gr = 10^5, Re = 1000, Pr = 0.71$

Number of Elements	Nu_r
5212	5.4875
16125	5.5401
25207	5.5613
39096 (Optimum)	**5.5741**
50331	5.5790

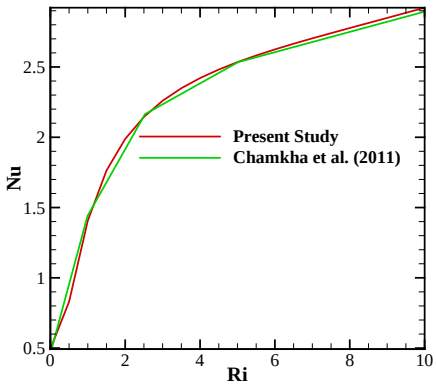

Figure 2. Validation of the present model with the work of Chamkha et al. (2011) at CT configuration, $Re = 200$ and aspect ratio= 0.2

3.2 Validation

It is necessary to validate the model with existing the literature before performing any numerical simulation. The present model is also validated with the work of Chamkha et al. (2011) at CT configuration for $Re = 100$. The

average Nusselt number along the cold wall versus Richardson number plot for the present study, and Chamkha et al. (2011) is in close agreement, which is illustrated in figure 2.

5. Results and Discussion

The numerical simulation is done for three different arrangements of the cooler. Grashof number (Gr) is fixed at 10^5 throghout the simulation. Richardson number (Ri) is varied from 0.1 to 10, and the Reynolds number is changed accordingly from 10^2 to 10^3.

To understand the thermal structure inside the room, three different values of Ri, 0.1, 1, and 10 are chosen, which are illustrated in figure 3. For Ri = 0.1, the forced convection is dominant. The temperature is mostly stratified near the active left and the right walls. As the natural convection effect is less, relatively cold air from the inlet distributes less uniformly around the room. Consequently, low temperature exists along the main flow trajectory of the cold air from the inlet to the outlet. Therefore, for case 3, the lower portion of the cavity is hotter than the other two scenarios. For Ri = 1, both natural convection and forced convection are equally influential. The cold inlet air mixes around the relatively hot air and becomes lighter, therefore moves a little upward. As a result, the outlet air's temperature is much higher than the cases at $Ri = 0.1$. The isotherms near the end of the right wall move towards the left for case 2 and case 3. On the contrary, case 1 has near-parallel isotherm lines near the right wall. The temperature gradient is relatively steep in the middle of the inner right wall for case 1, whereas for cases 2 and 3, the gradient is steep at the top of the inner right wall. The same phenomenon is also observed at $Ri = 0.1$.

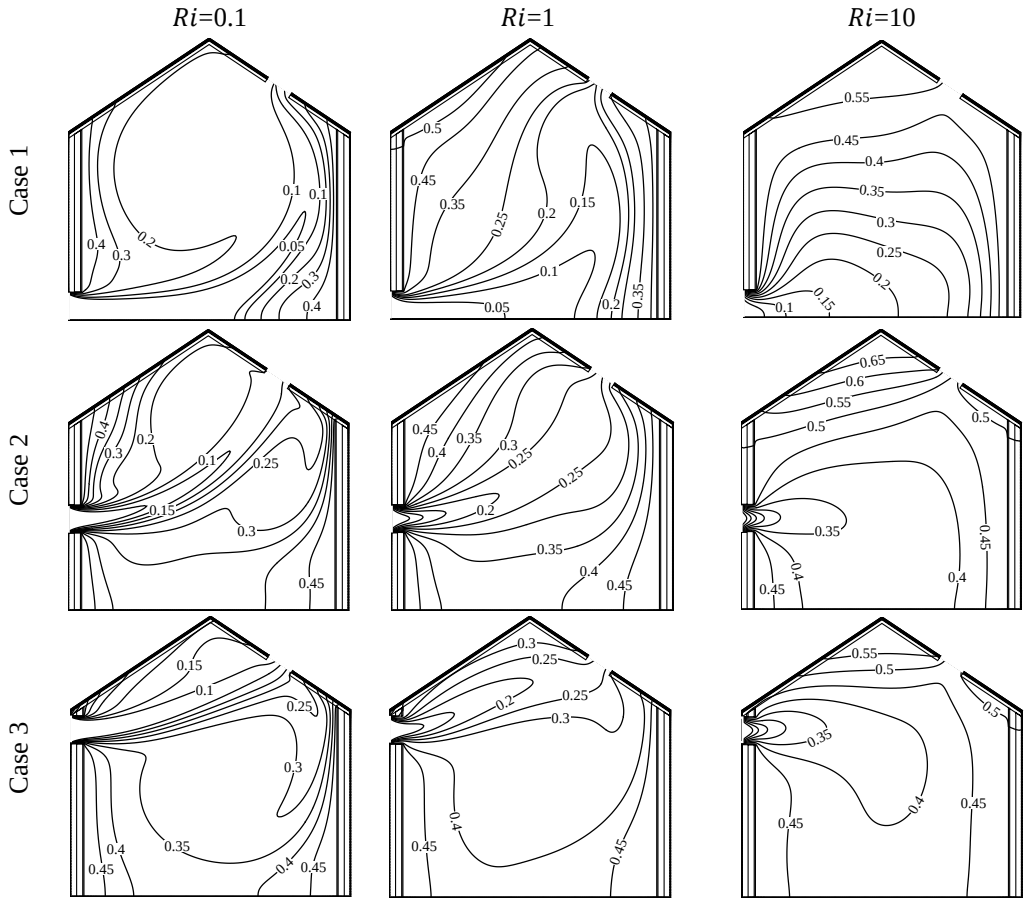

Figure 3. Isotherm plots for different cases of geometric configuration and different values of Richardson number

Natural convection is the primary dominant mode for Ri = 10. For this Richardson number, it is observed that that the cold air becomes hot and moves upward. Thus, the natural convection currents distribute the temperature more uniformly around the room. The outlet temperature is also higher because the inlet air mixes more across the spaces.

Figure 4 illustrates the streamline pattern inside the cavity. Streamlines visualization is critical to understand the flow behaviors. At Ri = 0.1, the forced convection mode is dominant; the flow tends to directly go from the inlet to the outlet. As the inlet velocity is much higher at Ri = 0.1 and the inlet-outlet distance is maximum for case 1, the flow moves almost horizontal at first and then vertically to the outlet, resulting in an L-bend type shape. In case 3, the open lines are mostly straight as the inlet and the outlet are in a minimum distance between the three scenarios. The natural convection effects are also less. However, owing to the existence of convection currents and buoyancy effects, two separate recirculating cells are formed on the two opposite sides of the open lines. A comparatively larger vortex cell is formed on the upper side, and a negligible vortex cell on the lower right side of the cavity is formed in case 1. In contrast, for case 3, a relatively large vortex cell is formed below the open lines, and a small one is formed above the open lines. For case 3, almost the similar size vortex cells are developed below and above the open lines. While relatively cold air sets open lines and the air above and below the open lines are relatively cooler, two separate recirculating areas are formed due to buoyancy forces. Hence, the vortex cells below and above the heated lines are circulating in opposite directions. At Ri = 1, both the forced convection and the natural convection mode of heat transfer are dominant. The inlet flow is greatly affected by buoyancy forces. The opens lines are slightly spread inside the cavity. For case 1, two separate vortex cells are formed above the open lines, and there isn't any vortex cell below it. For case 2, two different vortex cells are formed on the two opposite sides of the open lines, although the upper one is small in size, whereas only one vortex cell is found in case 3. The effect of spreading the open lines within the cavity is more noticeable at Ri=10, as the natural convection is more dominant. Though strong buoyancy force is favorable for producing strong vortex cells, the influence of expanding the open lines

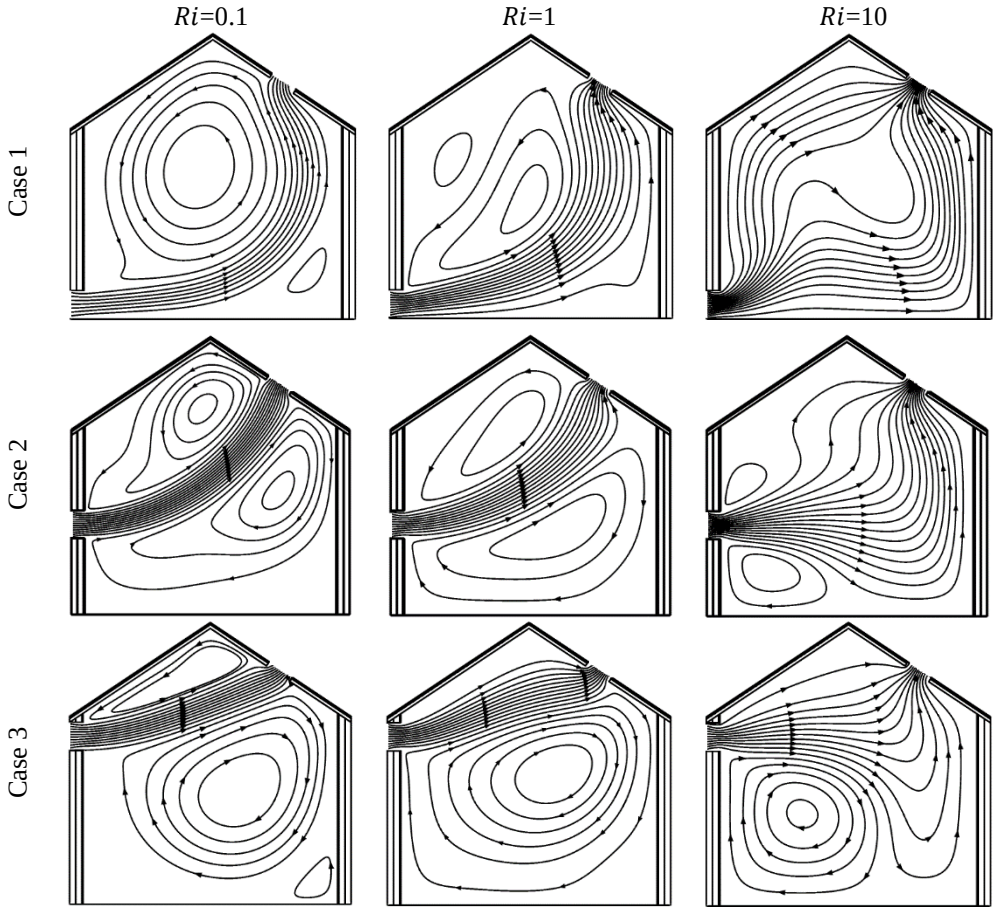

Figure 4. Streamline plots for different cases of geometric configuration and different values of Richardson number

across the cavity due to buoyancy is notable. Hence, for case 1, there is no vortex cell; the open lines spread throughout the cavity and prohibits any vortex formation. For case 2 and case 3, vortex cells are generated but are of small sizes.

The distribution of heatlines for three cases are illustrated in Figure 5. Heatlines inside the prismatic cavity gives a clear overview of the convective heat transport happening inside. Moreover, thermal mixing can also be understood from the heatline illustrations. As from the definition, it can be said that a lower Richardson number creates more turbulence, and thus, more heat transport occurs. In contrast to that, a higher Richardson number offers steady but less thermal mixing capability. The heatline illustrations exactly behave accordingly. Figure 5 depicts that at a high Reynolds number, vortices form, and heat is transferred more abruptly from the heated surfaces. At Ri = 0.1 and Ri=1, counter-clockwise vortices can be seen. Here, we could also observe that in case 2 and case 3, the chilled air quickly finds its way to the exit port. At a high flow of cold air (low Richardson number), the air could not find enough space to stay longer inside the cavity because of the geometry. From the heatline illustrations, it is observed that for case 1, better heat dissipation can be achieved. For case 1, regardless of Richardson numbers, the cold air circulates more inside the cavity, and so, greater mixing of cold air and heated air is possible. This phenomenon is also observed in the dimensionless average temperature of the air versus the Richardson number plots. From figure 7, case 1 experiences the coldest temperature. So, the cooler position is preferred to be at the bottom for better thermal mixing.

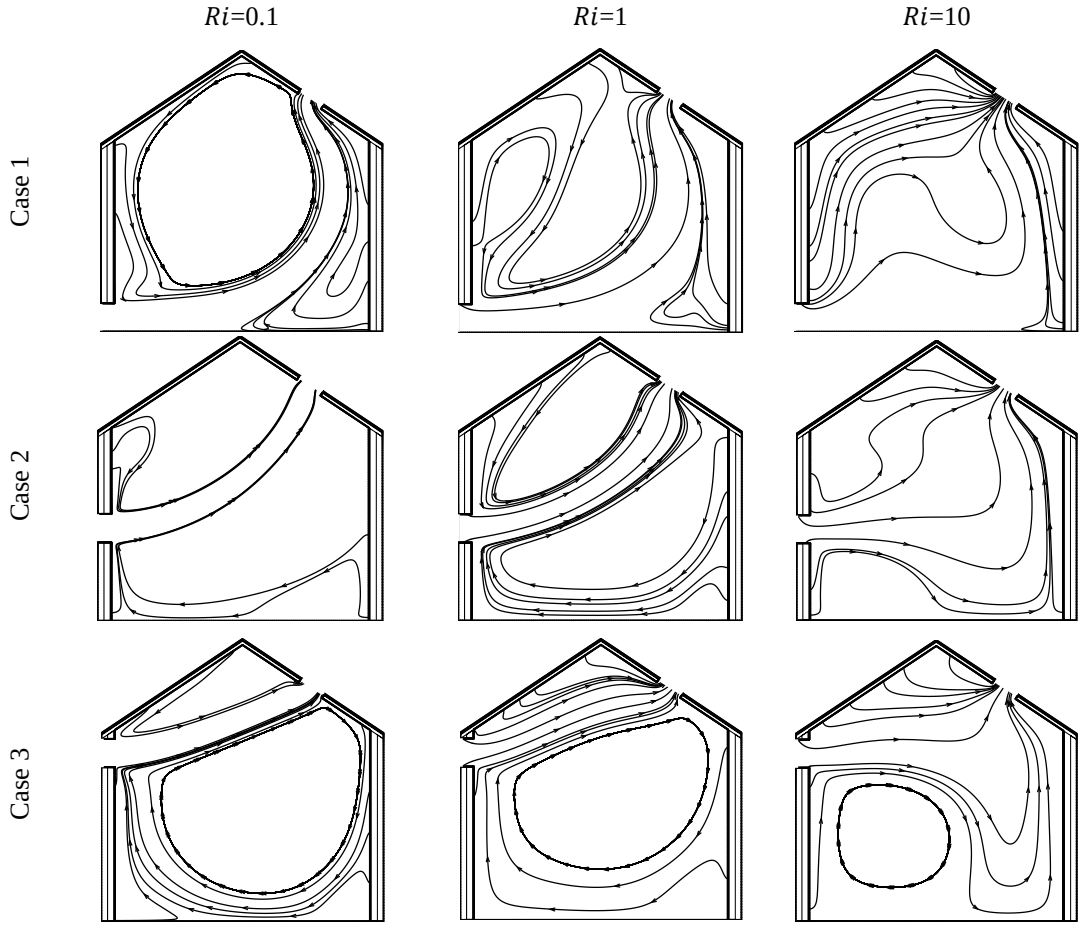

Figure 5. Heatline plots for different cases of geometric configuration and different values of Richardson number

Nusselt number indicates the ratio between conductive heat transfer and convective heat transfer performance. Figures6(a) and 6(b) illustrate the variation of Nusselt number with Richardson number or Reynolds number along the inner right wall and top inclined wall, respectively. Nusselt number along the inner top wall (Nu_t) is maximum at case 3 regardless of Reynolds number, which is predictable from isotherm lines and streamlines because the low-

temperature air from the inlet is concentrated around the top portion of the cavity and the temperature gradient from the inner inclined wall to the open streamlines are very steep. Hence, heat transfer from the inner inclined wall to the air is maximum due to the convections. Conversely, Nu_r is minimum at case 3 as the cold air accumulates less around the inner right wall. Increasing the forced convection effect increases the Nusselt number value in any case because forced convection stimulates the convection currents.

In figure 7(a), the variation of dimensionless average temperature in the air domain inside the room with Richardson number is illustrated. Cold air is supplied from the cooler, and the average temperature of the room drops. At low Ri number, the inlet velocity is more, and more cold air enters the room, resulting in a decrease of average dimensionless temperature. Hence, average room temperature increases with the increase of Richardson number for all three cases. For case 3, the cold air distributes ineffectively inside the room, as the inlet and the outlet are in a short distance compared to others. Therefore, the cold air enters and directly exits through the outlet; less mixing occurs with the air in the lower portion of the cavity, resulting in a higher average temperature for all Richardson numbers. In contrast, for case 1, the cold air has to flow from the lower portion to the upper right side of the cavity; the dimensionless average temperature of the fluid decreases significantly. For the same reasons, in case 2, the air's dimensionless average temperature is between case 1 and case 3 except for the high low Reynolds number, where the average temperature is the same for case 2 and case 3.

Figure 7(b) illustrates the temperature distribution effectiveness in relation to the Richardson number. From the figure, it is clear that case 1 has better temperature distribution effectiveness regardless of the value of the Richardson number; case 3 has the opposite. Temperature distribution effectiveness also increases with Richardson number except for some portions in case 1.

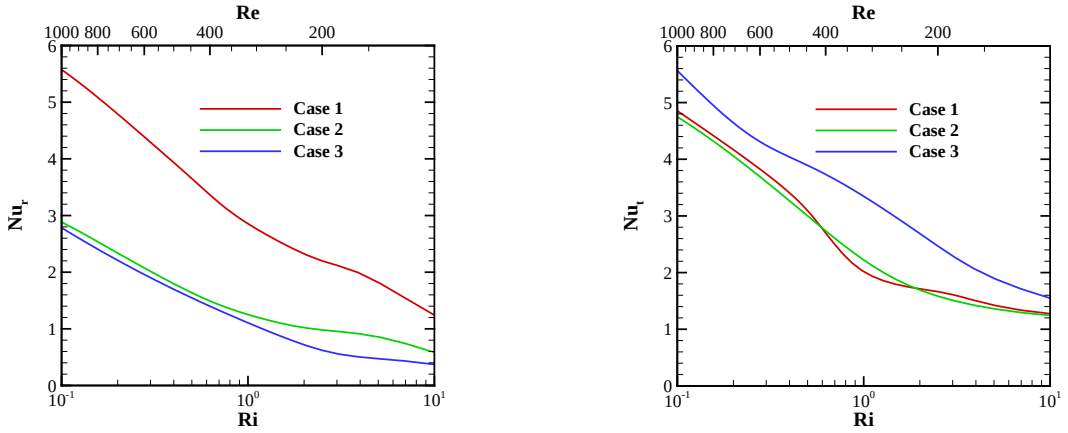

(a) (b)

Figure 6. Variation of average Nusselt number as a function of Richardson number at the (a) inner right wall, (b) inner top wall.

For case 1, during $Ri \approx 0.5$, ε_T suddenly starts to drop and reach a local minimum at $Ri \approx 0.9$, and then starts to increase and reach a maximum value at $Ri \approx 4$. At a low Ri , forced convection has the dominant effect, so the inlet air tends to move to the outlet without mixing with the existing room air, causing a decrease in ε_T values. Mixing of air by buoyancy forces is conducive to higher values of temperature distribution effectiveness.

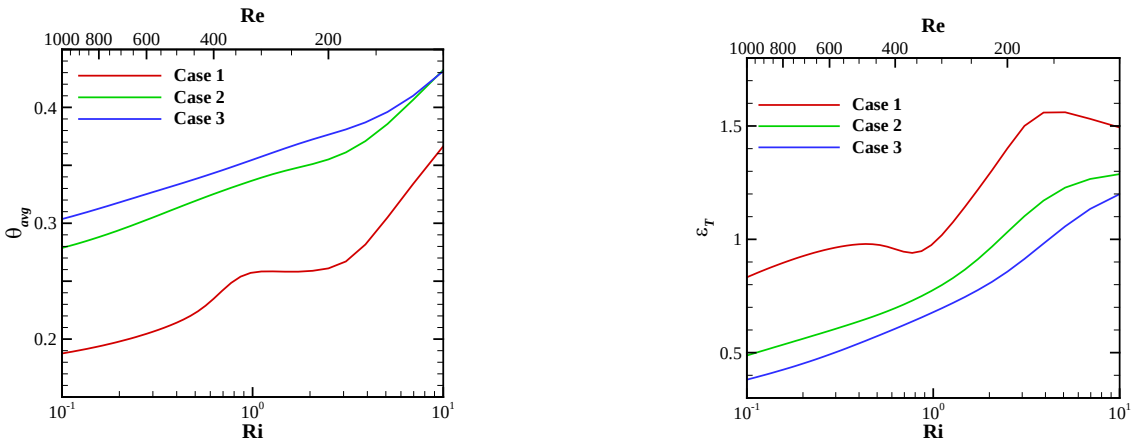

Figure 7. Variation of (a) dimensionless average temperature, (b) temperature distribution effectiveness, as a function of Richardson number

6. Conclusion

Numerical simulation of mixed convection heat transfer in a vented prismatic enclosure has been carried out in this study. The main target here was to find an optimum configuration. Based on the different plots, the following conclusions can be drawn:

- For any Richardson number, the average temperature inside the room is minimum for case 1. Hence, this geometric configuration is more suitable for the summer seasons. Low Richardson number ($Ri \approx 0.1$), or high inlet air velocity, exhibits minimum average temperature inside the room.
- Case 3 exhibits the maximum average temperature of the air. Hence, it is suitable for the winter seasons but might not be energy efficient. Case 2 also has a high average temperature and almost equal to that of case 3 at the high Richardson number.
- Temperature distribution around the room is better for case 1 than case 2 and case 3.
- The average Nusselt number along the inner right wall is maximum for case 1, whereas the average Nusselt number along the inner top wall is maximum for case 3.

Acknowledgements

The authors would like to express their appreciation to the Department of Mechanical Engineering, Bangladesh University of Engineering and Technology, for providing support and necessary facilities during the research process.

References

Manca, O., Nardini, S., Khanafer, K., and Vafai, K., Effect of Heated Wall Position on Mixed Convection in a Channel with an Open Cavity, *Numerical Heat Transfer; Part A: Applications*, vol. 43, no. 3, pp. 259–282, 2003.

Manca, O., Nardini, S., and Vafai, K., Experimental Investigation of Mixed Convection in a Channel with an Open Cavity, *Experimental Heat Transfer*, vol. 19, no. 1, pp. 53–68, 2006.

Alam, M. S., Rahman, M. M., Parvin, S., and Vajravelu, K., Finite Element Simulation for Heatline Visualization of Natural Convective Flow and Heat Transfer inside a Prismatic Enclosure, *International Journal of Heat and Technology*, vol. 34, no. 3, pp. 391–400, 2016.

Walid, W., Omri, A., and Nasrallah, S. B., Buoyancy Induced Heat Transfer and Fluid Flow Inside a Prismatic Cavity, *Int. Symp. on Convective Heat and Mass Transfer in Sustainable Energy, Tunisia*, pp. 1-15, 2016.

Hasan, A. B. M. R., Sagor, M. J. H., Barua, S., and Saha, S., Effect of Heating Condition on Entropy Generation of Conjugate Natural Convection in a Prismatic Enclosure, *AIP Conference Proceedings*, vol. 2121, pp. 030001, 2019.

Rahman, M. M., Alim, M. A., Mamun M. A. H., Chowdhury, M. K., and Islam, A. K. S. M., Numerical Study of Opposing Mixed Convection in a Vented Enclosure, *Network*, vol. 2, no. 2, pp. 25–36, 2007.

Aminossadati, S. M., and Behzad, G., A Numerical Study of Mixed Convection in a Horizontal Channel with a

Discrete Heat Source in an Open Cavity, *European Journal of Mechanics B/Fluids*, vol. 28, no. 4, pp. 590–598, 2009.

Shirvan, K. M., Mamourian, M., and Ellahi, M., Numerical Investigation and Optimization of Mixed Convection in Ventilated Square Cavity Filled with Nanofluid of Different Inlet and Outlet Port, *International Journal of Numerical Methods for Heat and Fluid Flow*, vol. 27, no. 9, pp. 2053–2069, 2017.

Carozza, A., Numerical Study on Mixed Convection in Ventilated Cavities with Different Aspect Ratios, *Fluids*, vol. 3, no. 1, pp. 11, 2018.

Gan, G., and Awbi, H. B., Numerical Simulation of the Indoor Environment, *Building and Environment*, vol. 29, no. 4, pp. 449–459, 1994.

Raji, A., and Hasnaoui, M., Mixed Convection Heat Transfer in Ventilated Cavities with Opposing and Assisting Flows, *Engineering Computations (Swansea, Wales)*, vol. 17, no. 5, pp. 556–572, 2000.

Hinojosa, J. F., Rodríguez, N. A., and Xamán, J., Heat Transfer and Airflow Study of Turbulent Mixed Convection in a Ventilated Cavity, *Journal of Building Physics*, vol. 40, no. 3, pp. 204–234, 2016.

Stavridou, A. D., and Prinos, P. E., Unsteady CFD Simulation in a Naturally Ventilated Room with a Localized Heat Source, *Procedia Environmental Sciences*, vol. 38, pp. 322–330, 2017.

Koufi, L., Younsi, Z., Cherif, Y. and Naji, H., Numerical Investigation of Turbulent Mixed Convection in an Open Cavity: Effect of Inlet and Outlet Openings, *International Journal of Thermal Sciences*, vol. 116, pp. 103–117, 2017.

Chamkha, A. J., Hussain, S. H., and Abd-Amer, Q. R., Mixed Convection Heat Transfer of Air Inside a Square Cavity with a Heated Horizontal Square Cylinder, *Numerical Heat Transfer, Part A: Applications*, vol. 59, no. 1, pp. 58-79, 2011.

Biographies

Rashadul Islam Ritu is a student of Mechanical Engineering (ME) at Bangladesh University of Engineering and Technology. He currently lives in Dhaka, Bangladesh. He passed his HSC from Notre Dame College and SSC from Ideal School and College. His research interest includes heat and mass transfer, computational fluid mechanics.

Enamul Hasan Rozin is a Bangladeshi citizen who is currently living in Dhaka, Bangladesh. He is pursuing his B. Sc. Engg. Degree in Mechanical Engineering at the Bangladesh University of Engineering and Technology. His research interests include heat and mass transfer, computational fluid mechanics, molecular dynamics, artificial neural networks (ANN). He has some publications at different international conferences.

Sumon Saha received his Ph.D. in Engineering from the University of Melbourne, Victoria, Australia, in 2014. He completed his B.Sc. and M.Sc. in Mechanical Engineering from Bangladesh University of Engineering and Technology (BUET), Dhaka, Bangladesh, in 2004 and 2007, respectively. His major field of study is the numerical analysis of problems of thermo-fluid. He is now working as an Associate Professor in the Department of Mechanical Engineering of Bangladesh University of Engineering and Technology (BUET). He already published more than 130 research papers in International Journals and Conference Proceedings and co-author of two books in the engineering field. His fields of interest are turbulent flows, computational fluid mechanics, computational heat transfer, and thermal post-buckling analysis. Dr. Saha is the editor of one international journal and a reviewer of several international conference proceedings and international journals. He is currently a senior member of the International Association of Computer Science and Information Technology (IACSIT), Singapore. Moreover, he is a life member of the Bangladesh Solar Energy Society. He has received many professional awards like the International Postgraduate Research Scholarship by the Australian federal government; Melbourne International Research Scholarship by the University of Melbourne; RHD Studentship by the University of Melbourne, and so on.

Sheikh Mohammad Shavik is an Assistant Professor of the Department of Mechanical Engineering at Bangladesh University of Engineering and Technology, Dhaka, Bangladesh. He completed his Ph.D. from the Department of Mechanical Engineering at Michigan State University, East Lansing, Michigan, USA, where his thesis work was on developing a multi-organ finite element modeling framework of the human heart with ventricular-arterial interactions. Before that, he received his Bachelor of Science and Master of Science degrees from the Department of Mechanical Engineering, BUET. His research interest includes computational mechanics, particularly modeling the human heart and cardiovascular system integrated with the clinical and experimental data, biomechanics, and developing computational models of Multiphysics problems.